Unveiling the X-ray polarimetric properties of LMC X-3 with IXPE, NICER, and Swift/XRT

Akash Garg, Divya Rawat, Mariano Méndez

Monthly Notices of the ROYAL ASTRONOMICAL SOCIETY

MNRAS **531,** 585–591 (2024) https://doi.org/10.1093/mnras/stae1198
Advance Access publication 2024 May 03

Unveiling the X-ray polarimetric properties of LMC X−3 with *IXPE*, *NICER*, and *Swift*/XRT

Akash Garg [1]★ Divya Rawat [1,2]★ and Mariano Méndez [3]★

[1] *Inter-University Center for Astronomy and Astrophysics, Ganeshkhind, Pune 411007, India*
[2] *Observatoire Astronomique de Strasbourg, Université de Strasbourg, CNRS, 11 rue de l'Université, F-67000 Strasbourg, France*
[3] *Kapteyn Astronomical Institute, University of Groningen, PO BOX 800, Groningen NL-9700 AV, the Netherlands*

Accepted 2024 May 1. Received 2024 May 1; in original form 2023 September 12

ABSTRACT

The incoming *Imaging X-ray Polarimetry Explorer* (*IXPE*) observations of X-ray binaries provide a new tool to investigate the underlying accretion geometry. Here, we report the first measurements of X-ray polarization of the extragalactic black-hole X-ray binary LMC X−3. We find a polarization fraction of ~ 3 per cent at a polarization angle of $\sim 135^{\circ}$ in the 2–8 keV energy band with statistical significance at the 7σ level. This polarization measurement significantly exceeds the minimum detectable polarization threshold of 1.2 per cent for the source, ascertained at a 99 per cent confidence level within the 2–8 keV energy band. The simultaneous spectro-polarimetric fitting of *Neutron Star Interior Composition Explorer*, *Swift*/X-Ray Telescope (XRT), and *IXPE* revealed the presence of a disc with a temperature of ∼1 keV and a Comptonized component with a power-law index of ∼2.4, confirming the soft nature of the source. The polarization degree increases with energy from ∼3 per cent in the 2–5.7 keV band to ∼9 per cent in the 5.7–8 keV band, while the polarization angle is energy independent. The observed energy dependence and the sudden jump of polarization fraction above 5 keV supports the idea of a static slab coronal geometry for the Comptonizing medium of LMC X−3.

Key words: accretion, accretion discs – polarization – X-rays: binaries – X-rays: individual: LMC X-3.

1 INTRODUCTION

Black hole X-ray binaries (BXB) are an exquisite class of astronomical systems in which a black hole accretes matter from a companion star and forms a planar structure known as an accretion disc. Such an accretion disc is a powerful source of electromagnetic radiation, emitting profusely in X-ray, optical, and radio wavelengths. During its outburst, the BXB transitions from a low-hard state (LHS, low flux of high-energy photons) to a high-soft state (HSS, high-flux of low-energy photons) via hard/soft intermediates states and sometimes, steep-power law (SPL) state (see Remillard & McClintock 2006; Motta et al. 2012). These states are characterized by varying proportions of count rate and flux hardness (Belloni et al. 2005; Belloni, Motta & Muñoz-Darias 2011, and references within). In the HSS, the spectrum is primarily characterized by an optically thick thermal component, often modelled as a multitemperature blackbody of temperature ∼1 keV (Shakura & Sunyaev 1973). Occasionally, a power-law component with a power-law index $\Gamma \geq 2$ is also observed alongside the thermal component (Méndez & van der Klis 1997; Done, Gierliński & Kubota 2007). In contrast, during the LHS, the X-ray spectrum exhibits a distinct feature attributed to Comptonization from an electron plasma with temperatures between 50 and 100 keV (Gilfanov 2010).

Over more than five decades, the X-ray spectro-timing analysis has proven to be an important tool to map the accretion region indirectly. Besides establishing the presence of a cold accretion disc for the soft component, different models such as the slab-corona model, patchy corona model, magnetized accretion ejection model, and more exist to justify the hard component in the spectra (Haardt & Maraschi 1993; Done et al. 2007, and references within). However, it is important to note that the inherent ambiguity regarding the nature of the Comptonizing medium cannot be fully resolved through X-ray spectro-timing analysis alone. Given this scenario, the X-ray polarization study offers an additional tool to break the existing degeneracies among the predictions for the accretion flow around the black hole. The linear polarization gives two extraparameters, polarization angle, and polarization degree, whose variations with energy and time can be predicted and checked against the observations.

Over the last few decades, numerous models have been proposed such as Monte-Carlo polarization simulations for a thermal accretion disc (Schnittman & Krolik 2009) and a wedge, clumpy or spherical corona (Schnittman & Krolik 2010). Krawczynski & Beheshtipour (2022) employed the KERRC model to determine polarization fractions within geometrically thin discs and examined the impact of varying coronal shapes. Poutanen, Veledina & Beloborodov (2023) applied radiative transfer simulations on the polarization spectrum for static and dynamical coronal regions. Podgorný et al. (2022) explored the effects of relativistic polarization using the KYNSTOKES code for lamp-post corona model. Furthermore, Zhang, Dovčiak & Bursa (2019) employed the MONK code to investigate Comptonization within the framework of Kerr space–time. Besides these, there are

★ E-mail: akashgarg_16@yahoo.co.in (AG); rawatdivya838@gmail.com (DR); mariano@astro.rug.nl (MM)

a few more studies that probe the accretion geometry in BXB using spectro-polarimetric signals. The launch of the *IXPE* (Imaging X-ray Polarimetry Explorer) mission provides the opportunity to test these models. Therefore, a comprehensive polarimetric study is necessary to untangle the geometry of the accretion and Comptonizing medium within these systems.

The recent *IXPE* observations of the BXB 4U 1630−47 have provided intriguing results. A polarization fraction of ∼ 8 per cent in the HSS (Kushwaha et al. 2023; Ratheesh et al. 2023; Rawat, Garg & Méndez 2023b) and ∼ 7 per cent in the SPL state (Rodriguez Cavero et al. 2023; Rawat, Garg & Méndez 2023a) was observed. This observed high-polarization fraction in the HSS has captured the attention of X-ray astrophysicists, as it defies explanations within the framework of contemporary models (Schnittman & Krolik 2010; Taverna et al. 2020; Krawczynski & Beheshtipour 2022). Similarly, using *IXPE*, Krawczynski et al. (2022) has reported a polarization fraction of 4 per cent in the hard state of Cygnus X−1, which is unusual for a low-inclination source assuming polarization is due to electron scattering.

Motivated by the recently reported high-polarization fraction for BXB in the high-soft state, we explore the polarimetric properties of LMC X−3 in this paper. LMC X−3 is a black hole X-ray binary source discovered in the Large Magellanic Cloud with Uhuru (Leong et al. 1971). The binary system has an inclination angle of ∼70° (Orosz et al. 2014). After its discovery, the spectral analysis by White & Marshall (1984) showed that LMC X−3 has an unusual soft X-ray spectrum, implying that the source is in the soft state for most of the time, comprising of an ultrasoft and a high-energy component. Later, LMC X-3 was also observed to undergo brief low/hard states (LHS, defined by simple power-law, Boyd et al. 2000; Wilms et al. 2001; Bhuvana, Radhika & Nandi 2022) and anomalous low states (Smale & Boyd 2012; Torpin et al. 2017). Fender & Hendry (2000) conducted a radio survey on persistent BXB sources and reported no radio counterpart of LMC X−3, which could be attributed to either the distant location of the source (∼48 kpc, Orosz et al. 2014) or its unusually soft spectrum. The dimensionless spin parameter of the black hole in this source, using different missions, is reported to be in the range ∼0.19–0.24 (Steiner et al. 2014; Jana et al. 2021; Bhuvana et al. 2022).

For highly inclined sources, if the polarization is due to electron scattering, then a high-polarization fraction is expected with the polarization angle aligned parallel to the disc plane (Chandrasekhar & Breen 1947; Chandrasekhar 1960; Sobolev 1963). The high-inclination angle and the fact that LMC X−3 spends most of its time in the soft state make it an excellent candidate for a polarimetric study. The subsequent sections of this paper are organized as follows: Section 2 covers the observations and data reduction methods, Section 3 presents polarimetric and spectro-polarimetric findings, and in Section 4 we conclude with interpretations and implications of our results for LMC X-3.

2 OBSERVATION AND DATA REDUCTION

In this work, we have used Neutron Star Interior Composition Explorer (*NICER*), *Swift*/XRT, and *IXPE* observations of the source LMC X−3 taken during 2023 July. The observation details with each instrument are given in Table 1, and the data reduction techniques are briefly discussed in the next subsections.

Table 1. Observation log for LMC X−3. The columns are the Instruments used, their ObsID, the observation's start and end date, and the exposure times.

Instrument	ObsID	Tstart (MJD)	Tstop (MJD)	Exposure (s)
NICER	6101010115	60128.67	60128.81	630
Swift/XRT	00089714001	60134.81	60134.83	1244
	00089714002	60139.12	60139.70	1772
	00089714003	60145.06	60145.20	1928
IXPE	02006599	60132.78	60145.60	561925

2.1 *NICER*

We have analysed observations of LMC X−3 with the *NICER* (Gendreau, Arzoumanian & Okajima 2012) on 2023 July 03. *NICER*'s XTI (X-ray Timing Instrument; Gendreau et al. 2016) covers the 0.2–12.0 keV band and has an effective area of >2000 cm^2 at 1.5 keV. The energy and time resolutions are 85 eV at 1 keV and 4 × 10^{-8} s, respectively. We have applied the standard calibration process and screening using the NICERL2[1] task. Further, the grouped spectrum is extracted using NICERL3,[2] which also applies systematic errors and quality flags to the spectrum. In addition, NICERL3 also creates ancillary (ARF), response (RMF), and background files (for the 3C50 model) using CALDB version 20221001.[3]

2.2 *Swift*/XRT

Swift/X-Ray Telescope (XRT) has observed the LMC X−3 in the window mode for three epochs between 2023 July 09 and 2023 July 20. *Swift*/XRT (Burrows et al. 2005) is an X-ray Imaging Telescope that operates in a narrow energy band of 0.2–10 keV with an effective area of ∼125 cm^2 at 1.5 keV. We have used XRTPIPELINE to extract the clean event files which are then used to extract the lightcurve using the XSELECT (V2.5b) package of HEASOFT version 6.32.1.[4] Utilizing an online *Swift*/XRT tool BUILD SWIFT-XRT PRODUCTS[5], we have created a single averaged spectrum from the three epochs along with ancillary response (arf) and response (rmf; see Evans et al. 2009) files. We have considered grade 0–2 events for the source spectra as the Windowed Timing (WT) mode data should not be affected by pile-up for source count below 100 c s^{-1} (Romano et al. 2006).

2.3 *IXPE*

IXPE is a recently launched X-ray polarimetry observatory developed by NASA in collaboration with the Italian Space Agency. It can measure the polarization properties of multiple X-ray sources in the energy band of 2–8 keV. Besides polarization, *IXPE* also captures the spatial, temporal, and spectral aspects of X-ray photons (Manfreda 2020; Baldini et al. 2021; Di Marco et al. 2022; Weisskopf et al. 2022). *IXPE* has observed the source LMC X−3 from 2023 July 07 to 2023 July 20 for a total exposure of ∼562 ks. Fig. 1 shows the *NICER* (top panel) and *Swift*/XRT (bottom panel) lightcurves in the 0.2–12 keV and 0.3–8 keV bands, respectively along with the simultaneous 2–8 keV averaged *IXPE* lightcurve (top panel)

[1] https://heasarc.gsfc.nasa.gov/docs/nicer/analysis_threads/nicerl2/
[2] https://heasarc.gsfc.nasa.gov/docs/nicer/analysis_threads/nicerl3-spect/
[3] https://heasarc.gsfc.nasa.gov/docs/heasarc/caldb/nicer/
[4] https://heasarc.gsfc.nasa.gov/lheasoft/download.html
[5] https://www.swift.ac.uk/user_objects/

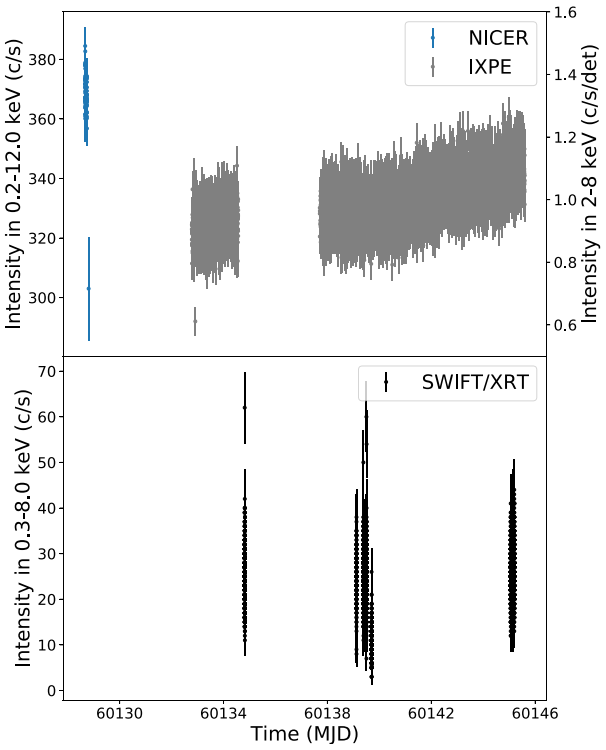

Figure 1. Top and bottom panels show the *NICER* (10 s bin), *IXPE* (100 s bin), and *Swift*/XRT (1 s bin) light curves of LMC X−3 in the 0.2–12, 2–8, and 0.3–8 keV bands, respectively.

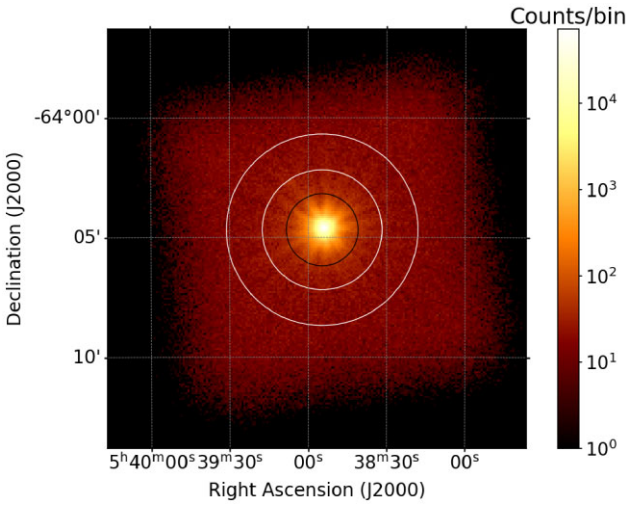

Figure 2. *IXPE* count map of detector DU1. The innermost and the two outer circles on the image show the circular source and annular background regions of LMC X−3 respectively.

extracted for the source region from all three detectors. We note here that the *NICER* observation is not simultaneous with *IXPE* but we still consider it for spectro-polarimetric analysis owing to minimal changes in source flux and spectral shape during the observation period.

We used the *IXPE* level-2 event files for all the detector units (DU) obtained directly from the High Energy Astrophysics Science Archive Research Center (HEASARC) archive. We begin by extracting and plotting the *IXPE* count image of event files using XSELECT and DS9, respectively, to choose the appropriate source and background regions as we show in Fig. 2 (for more details, see Podgorný et al. 2023). Further, we employ these regions (a circle of radius 1.5 arcmin for source and an annulus of inner and outer radii of 2.5 and 4 arcmin, respectively, for the background) in the XPSELECT tool of IXPEOBSSIM 30.2.2[6] (Baldini et al. 2022) to produce the cleaned source and background event files for all DUs. Then, we bin the event files using different algorithms of XPBIN (Kislat et al. 2015) to extract the polarization properties of the source. The emission model-independent polarization angle (PA) and polarization degree (PD) are estimated using the PCUBE method whereas XSPEC readable count I and Stokes Q and U spectra are created utilizing the algorithms PHA1, PHAQ, and PHAU, respectively, for all units in the 2–8 keV energy range. We have used the unweighted method and response matrices v012 of IXPEOBSSIM to produce all the polarization products.

We have rebinned I, Q, and U using FTGROUPPHA where the I spectrum is grouped using an optimal binning algorithm employing the response file. Subsequently, Stokes spectra are grouped using the I spectrum as a template file. We simultaneously fit the count spectra from *NICER* (in the 0.3–8 keV) and *Swift*/XRT (in the 0.4–5 keV) and Stokes spectra (Q, U) from *IXPE* (in the 2–8 keV) using the X-ray spectral fitting package XSPEC version 12.13.1.

[6]https://ixpeobssim.readthedocs.io/en/latest/overview.html

3 RESULTS

We carry out the standard model-independent (PCUBE) and spectro-polarimetric (XSPEC) approach to study the polarization properties of LMC X−3. In the PCUBE method, the Stokes parameters (I, Q, and U) are calculated by summing over the observed photoelectric emission angle for each *IXPE* event from which one can recover the polarization angle (PA) and polarization degree (PD) using usual formulae [see equations (21) and (22) in Kislat et al. 2015]. In the XSPEC method, polarization models like POLCONST, POLPOW or POLLIN are used along with basic radiative models to fit the count and Stokes spectra to determine the values of PA and PD.

3.1 Polarization properties using PCUBE

In the full *IXPE* energy range of 2–8 keV, we estimate a polarization degree of 2.9 ± 0.4 per cent ($>7\sigma$ significant) at a polarization angle of $135.1^\circ \pm 3.8^\circ$ ($>7\sigma$ significant) for the source. We have combined the measurements of all the detectors to improve the confidence interval over PA and PD of the observation. Our results are consistent with Majumder et al. (2024) and Svoboda et al. (2024), which have been reported simultaneously with this work. The polarization is well above the minimum detectable polarization (MDP_{99}) of 1.2 per cent for the source at a 99 per cent confidence interval. Fig. 3 shows the 1σ, 2σ, and 3σ confidence contour plots for PA and PD in the 2–8 keV band. The values of the polarization parameters are listed in Table 2. Unless stated, the reported error on each parameter is at the 1σ confidence level.

Further, we extract the polarization properties in four energy bands using the PCUBE algorithm and summed the values for each detector for accuracy. It is apparent from Fig. 4 that the PD is energy-dependent. Upto 5.66 keV the PD remains constant around 3 per cent through the first three energy bands, but increases significantly to ∼9 per cent in the 5.66–8 keV band. The values of polarization parameters along with their statistical significance and MDP_{99} are

Table 2. The PD and PA for LMC X−3 using all DUs were extracted using the PCUBE algorithm. The statistical significance of PD within each energy band is given in brackets alongside each PD value. The statistical significance of all the PA values is well above 7σ.

Energy (keV)	2–8	2–2.83	2.83–4.00	4.00–5.66	5.66–8.00
PD (per cent)	2.9 ± 0.4 (7.3σ)	2.5 ± 0.6 (4.2σ)	2.8 ± 0.5 (5.6σ)	3.3 ± 0.9 (3.7σ)	8.9 ± 2.5 (3.6σ)
PA (deg)	135.1 ± 3.8	136.2 ± 6.7	130.5 ± 5.5	141.6 ± 8.1	134 ± 8
MDP_{99} (per cent)	1.2	1.7	1.6	2.8	7.4

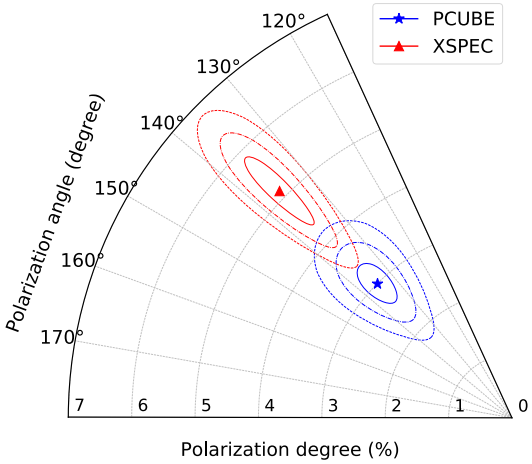

Figure 3. Contour plots of PA and PD of LMC X−3 in the 2–8 keV band with events from all DUs summed up using the PCUBE algorithm, and the XSPEC fitting method. The 3 contours represent confidence levels of 68.27, 95.45, and 99.73 per cent.

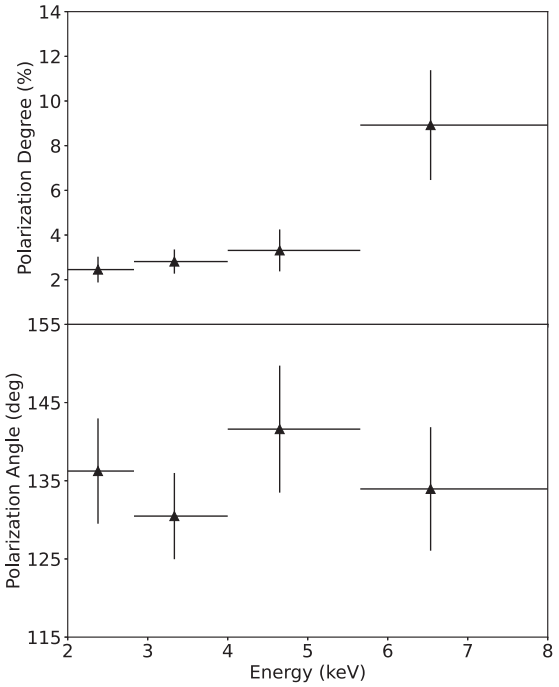

Figure 4. The PD (top panel) and PA (bottom panel) of LMC X−3 as a function of energy with events from all DUs summed up using the PCUBE algorithm.

listed in Table 2. The PA, on the other hand, is ∼135° and energy-independent. We also check the time evolution of PA and PD by dividing the data into seven almost equal time bins and running the algorithm for each. As shown in Fig. 5, we can measure the PA and PD significantly only in two time bins. Thereby, it will require longer exposures to determine any significant variations in the PD and PA with time.

3.2 Spectro-polarimetric fitting using XSPEC

We start by exploring the radiative properties of LMC X−3 by modelling only the *NICER* (0.3–8 keV) and *Swift*/XTI (0.4–5 keV) spectra simultaneously. We first fit the spectra with the model combination CONSTANT∗TBFEO∗(DISKBB + POWERLAW) with abundances from Wilms, Allen & McCray (2000) and cross-sections from Verner et al. (1996). The multiplicative factor CONSTANT accounts for the cross-calibration factor between *NICER* and *Swift*/XTI spectra. The TBFEO model describes the interstellar absorption and is similar to TBABS but allows to vary the oxygen and iron abundances of the interstellar absorber. The DISKBB and POWERLAW components describe the thermal disc and non-thermal Compton emissions from the source. The fitting gives a χ^2 of 312 for 276 d.o.f. For *NICER*, we use the systematics as obtained from NICERL3-SPECT, whereas, for *Swift*/XRT, we have taken a systematic error of 3 per cent. Letting the O abundance free, it could be constrained well to a value of ∼0.55 times the solar abundance. To check if a physical model like NTHCOMP can be used to characterize the high-energy emission, we fit the data with another model combination, CONSTANT∗TBFEO∗(DISKBB + NTHCOMP). This yields a χ^2 of 403 for 277 d.o.f, poorer than the previous case, and thereby we refrain from using this model for further spectro-polarimetric fitting.

Next, we fit the *I* spectra from *NICER* and *Swift*/XRT and the *Q*, and *U* spectra from *IXPE* simultaneously. We first try the model combination of CONSTANT∗POLCONST∗TBFEO∗(DISKBB + POWERLAW) where POLCONST is a multiplicative constant, energy-independent polarization model. This gives a χ^2 of 479 for 362 d.o.f. We have not taken any systematic error for *IXPE* spectra, and all the parameters were free during the fitting. The PA and PD values are inconsistent with the PCUBE results. This is expected, as we saw in the last section that the polarization degree is energy dependent.

Afterwards, we try the model CONSTANT∗POLPOW∗TBFEO∗(DISKBB + POWERLAW) where POLPOW is a multiplicative, power-law energy-dependent polarization model. During fitting, we have frozen $\psi_{\rm index}$ to zero because of the energy independence of the polarization angle. The χ^2 for the best-fit comes out to be 412 for 361 d.o.f, better than the previous model. All the best-fitting parameters are given in Table 3, and the simultaneously fitted *I*, *Q*, and *U* spectra for all detectors along with residuals are shown in Fig. 6. The estimated value of PA is 135.7° ± 3.7°, and of PD[7] is 5.1 ± 3.4 per cent,[8]

[7]We estimate the PD by integrating the POLPOW model in the 2–8 keV band.
[8]3σ error bar.

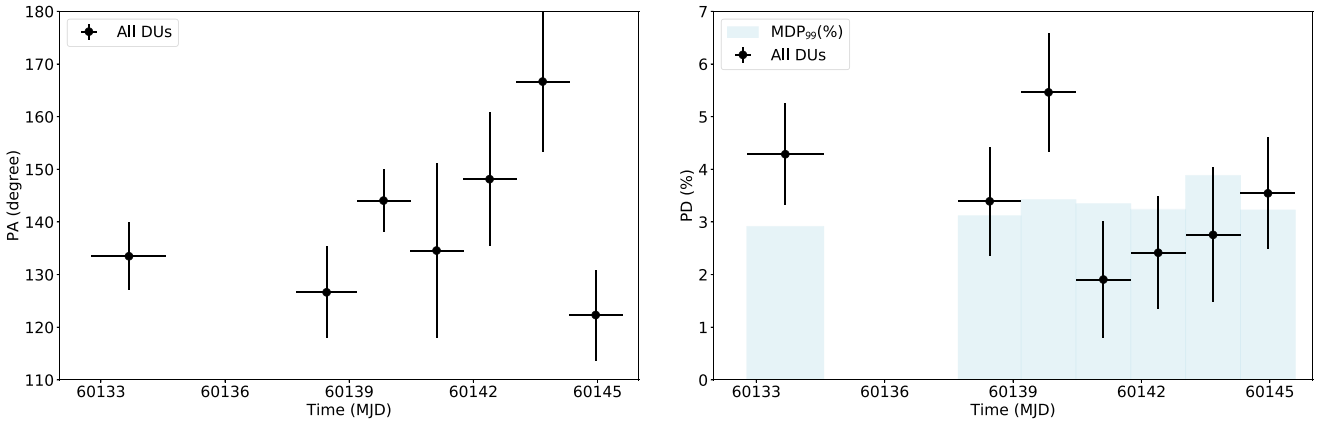

Figure 5. The PA (Left panel) and PD (Right panel) of LMC X−3 as a function of time with events from all DUs summed up using the PCUBE algorithm. The shaded region in the Right panel represents MDP_{99} for each time bin.

Table 3. *NICER*, *Swift*/XRT, and *IXPE* best-fitting spectral parameters for LMC X−3 with the model CONSTANT∗POLPOW∗TBFEO∗(DISKBB + POWERLAW).

Component	Parameter	Value
polpow	$A_{\rm norm}$ (10^{-3})	5.4 ± 3.8
polpow	$A_{\rm index}$	-1.4 ± 0.5
polpow	$\psi_{\rm norm}$ (deg)	135.7 ± 3.7
TBfeo	$N_{\rm H}$ (10^{20} cm^{-2})	5.99 ± 0.46
TBfeo	O	0.57 ± 0.15
powerlaw	Γ	2.4 ± 0.1
powerlaw	norm (10^{-2})	2.5 ± 0.3
powerlaw	Flux[a] (10^{-10} erg cm^{-2} s^{-1})	1.20 ± 0.03
diskbb	$kT_{\rm in}$ (keV)	1.062 ± 0.008
diskbb	norm	24.6 ± 0.64
Total flux[a]	(10^{-10} erg cm^{-2} s^{-1})	7.53 ± 0.02
χ^2/dof		412/361

[a]Total unabsorbed flux in the 0.3–8 keV range.

which are consistent with PCUBE results within the error bars as shown in Fig. 3.

4 DISCUSSION AND SUMMARY

We report the first measurement of X-ray polarization in the soft state of the extragalactic BXB source LMC X−3 using *IXPE* in the 2–8 keV energy band. The PD is ∼3 per cent at a PA of ∼135°. The lightcurves from *IXPE*, *NICER,* and *Swift*/XRT show no significant variation of the count rate of LMC X−3 across the 2–8, 0.2–12, and 0.3–8 keV bands, respectively (see Fig. 1). Simultaneous *NICER* and *Swift*/XRT spectra of LMC X−3 exhibit multitemperature blackbody emission peaking at around 1 keV. The spectra also display a significant contribution from a thermal Comptonization component with a power-law index of approximately 2.4. The PD increases from ∼3 per cent in the 2–2.83 keV band to ∼9 per cent in the 5.66–8.00 keV band while the PA shows no dependence on energy (see Fig. 4). The energy dependence of the PD is similar to what has been reported for the BXB sources 4U 1630−47 (Kushwaha et al. 2023; Ratheesh et al. 2023; Rodriguez Cavero et al. 2023; Rawat et al. 2023a, b) and Cygnus X−1 (Krawczynski et al. 2022).

Employing radiative transfer simulations, Poutanen et al. (2023) computed the dependence of the PD with the inclination angle of the source for both a slab coronal model and a hot inner flow model, accounting for relativistic plasma effects. In the static slab corona model, where the corona covers the cold accretion disc and seed photons originate from it, they found that the PD reaches approximately 4 per cent for high-inclination sources (i.e. $i \sim 70°$) at 4 keV (see top panel of fig. 3 in Poutanen et al. 2023). Considering a high-inclination angle of LMC X−3 (Orosz et al. 2014), our observed polarization fraction of around 3 per cent (within a 3-sigma range, as shown in Fig. 3) is consistent with this result. Furthermore, we have detected a significant increase in the PD above 5 keV, as illustrated in Fig. 4 and tabulated in Table 2. Poutanen et al. (2023) also found an increase in the PD with energy for the case of the static corona for two different inclination angles, $i = 30°$ and $i = 60°$, and a specific set of disc and coronal parameters, $kT_{\rm bb} = 0.1$ keV, $kT_{\rm e} = 100$ keV, and $\Gamma = 1.6$. They show that the PD rises from ∼2 per cent to ∼5 per cent for $i = 60°$ in the *IXPE* band of 2–8 keV. Our observations indicate an increase of the PD of up to around 9 per cent, with a lower limit of 6.5 per cent within the same energy range, which is closer to what Poutanen et al. (2023) found. The minor difference between their results and ours could be due to the spectral parameters we estimated, which could change the number of scatterings at higher energies and consequently influence the PD value (Poutanen et al. 2023). Moreover, the slab coronal model is known to generate excessively soft X-ray spectra (Stern et al. 1995), and LMC X−3 also possesses an unusually soft X-ray spectrum comprising an ultrasoft and a high-energy component during its soft state (White & Marshall 1984). So, the spectral analysis also gives a hint for slab-like corona geometry, but observed polarization measurements along with the simulation results provide additional support.

Schnittman & Krolik (2010) also calculated X-ray polarization for accreting black holes for three different coronal geometries, and they observed a consistent trend of increasing PD and a transition from horizontal to vertical polarization across all the geometries. However, they also found that in the spectral state characterized by an inner disc temperature of 1 keV and an electron temperature of 100 keV, the level of polarization is ∼3 per cent for sandwich geometry but lower for the clumpy and spherical coronae at high-inclination angles. It should be noted that their sandwich geometry is somewhat like the slab-like corona, which we argue is a likely geometry to explain the polarization of LMC X−3.

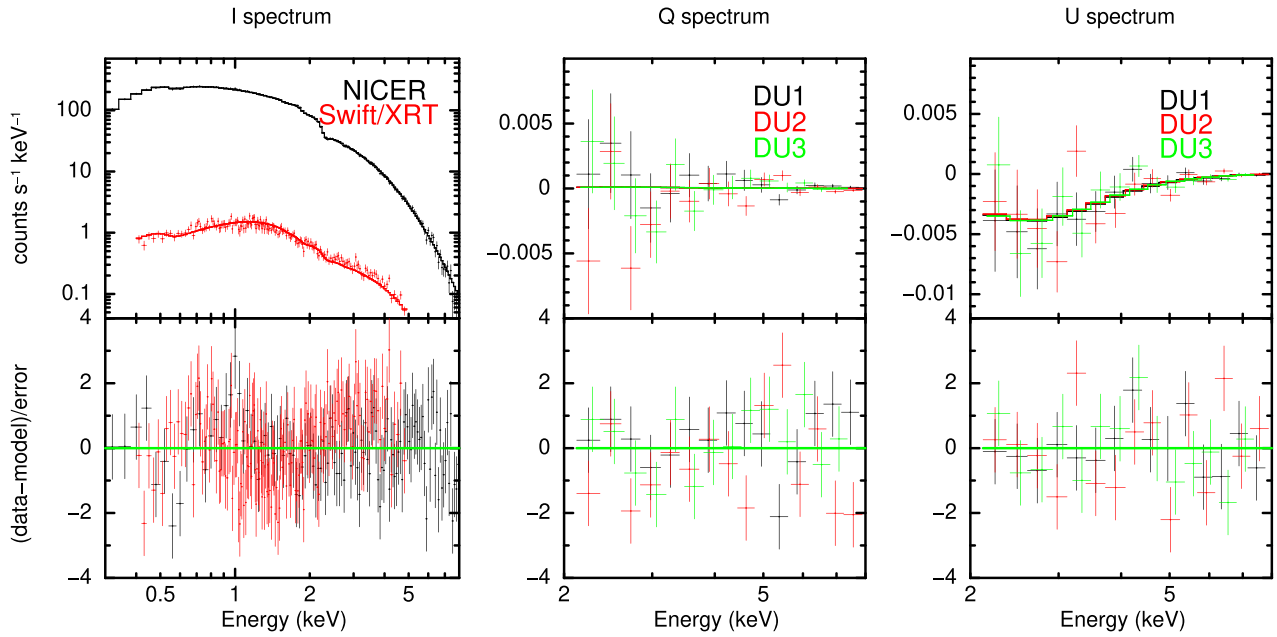

Figure 6. The top left panel presents the results of the simultaneous fits to the *NICER* and *Swift*/XRT spectra, while the top middle and top right panel shows the *IXPE* Stokes spectra, Q, and U, respectively. The model used for fitting the data is POLPOW∗TBFEO∗(DISKBB + POWERLAW). The bottom panels display the residuals of the best-fitting model. For the best-fitting parameters, refer to Table 3.

Poutanen & Svensson (1996) highlighted that the reversal of the PD sign is a distinctive characteristic associated with the slab corona geometry. Here, the positive polarization indicates that the electric field vector is predominantly perpendicular to the slab corona, while negative polarization indicates that the electric field vector is predominantly parallel to the slab corona. Using the radiative transfer code of Poutanen et al. (2023) and considering a slab coronal geometry for seed photons temperature of $kT_{bb} = 0.8$ keV and Comptonizing medium of temperature $kT_e = 10$ keV, Podgorný et al. (2023) found that the PD changes sign from negative to positive at ∼5 keV (see fig. 8 of Podgorný et al. 2023). They suggest that the overall polarization arises from emission polarized in both the parallel and perpendicular directions, which causes a low PD in the system. However, in this work, we found that the polarization fraction remains at ∼3 per cent in the 2–5.66 keV band and increases to ∼9 per cent in the 5.66–8 keV band as quoted in Table 2. But, it is to be noted that the temperature of the seed photons, the Comptonizing medium, and the geometry of the coronal medium significantly influence the energy at which the sign reversal of the PD occurs here and thereby could be the cause of the absence of any sign reversal in our observations.

In the context of BXBs, assuming a static hot inner flow geometry, the anticipated polarization level is approximately 7–8 per cent at 4 keV, as demonstrated in the middle and bottom panels of fig. 3 in Poutanen et al. (2023). Furthermore, the polarization fraction can be enhanced when accounting for relativistic plasma. Poutanen et al. (2023) has shown that for Cygnus X−1, the polarimetric results cannot be explained through static coronal models, and thus an outflowing plasma with a mildly relativistic velocity is required. Dexter & Begelman (2023) has also proposed bulk Comptonization of coronal emission in a mildly relativistic wind or jet for Cygnus X−1 to explain the observed polarization fraction. Unlike Cygnus X−1, the static slab corona geometry provides a successful explanation for the polarimetry findings in the case of LMC X−3. It is worth noting that the possibility of an enhancement of the PD due to disc winds, as reported by Kosenkov et al. (2020) for the black-hole binary MAXI J1820+070, or PD suppression due to disc winds, as suggested by Tomaru, Done & Odaka (2023) for 4U 1630−47, cannot be ruled out. Majumder et al. (2024) proposed that a direct and reflection emission in the partially ionized atmosphere (as suggested by Ratheesh et al. 2023, for the black hole source 4U 1630+47) could be the cause of the observed energy-dependent polarization. However, in the spectra of LMC X−3, we have not detected any signature of relativistic disc winds which can show the presence of any ionized atmosphere.

If disc self-irradiation produces polarization, the PA should align with the jet axis, i.e. perpendicular to the disc plane in BXBs (Schnittman & Krolik 2009). Studies on Cygnus X−1 conducted by Chauvin et al. (2018) and Krawczynski et al. (2022) utilizing *PoGO+* and *IXPE* observations, respectively, have confirmed the alignment of the polarization angle with the radio jet. Similarly, optical polarimetry conducted by Kosenkov et al. (2020) has indicated that the polarization angle aligns with the jet axis for MAXI J1820+070 in the rising hard state. Unfortunately, for LMC X−3, the jet angle is unknown as no radio counterpart has been reported (Fender & Hendry 2000), so we cannot make any comparison.

ACKNOWLEDGEMENTS

We are grateful to an anonymous reviewer for their constructive comments, which helped us significantly improve the quality of the manuscript. This work used data from the UK Swift Science Data Centre at the University of Leicester. This research has made use of data and/or software provided by the High Energy Astrophysics Science Archive Research Center (HEASARC), which is a service of the Astrophysics Science Division at NASA/GSFC. DR acknowledges Centre National de la Recherche Scientifique (CNRS) for financial support. MM acknowledges support from the

research program Athena with project number 184.034.002, which was (partly) financed by the Dutch Research Council (NWO).

DATA AVAILABILITY

The *NICER*/XTI, *Swift*/XRT, and *IXPE* observations used in this work are available at the HEASARC website.

REFERENCES

Baldini L. et al., 2021, Astropart. Phys., 133, 102628
Baldini L. et al., 2022, SoftwareX, 19, 101194
Belloni T., Homan J., Casella P., van der Klis M., Nespoli E., Lewin W. H. G., Miller J. M., Méndez M., 2005, A&A, 440, 207
Belloni T. M., Motta S. E., Muñoz-Darias T., 2011, Bull. Astron. Soc. India, 39, 409
Bhuvana G. R., Radhika D., Nandi A., 2022, Adv. Space Res., 69, 483
Boyd P. T., Smale A. P., Homan J., Jonker P. G., van der Klis M., Kuulkers E., 2000, ApJ, 542, L127
Burrows D. N. et al., 2005, Space Sci. Rev., 120, 165
Chandrasekhar S., 1960, Radiative Transfer. Dover Publications, New York
Chandrasekhar S., Breen F. H., 1947, ApJ, 105, 435
Chauvin M. et al., 2018, Nat. Astron., 2, 652
Dexter J., Begelman M. C., 2023, MNRAS, 528, L157
Di Marco A. et al., 2022, AJ, 164, 103
Done C., Gierliński M., Kubota A., 2007, A&AR, 15, 1
Evans P. A. et al., 2009, MNRAS, 397, 1177
Fender R. P., Hendry M. A., 2000, MNRAS, 317, 1
Gendreau K. C., Arzoumanian Z., Okajima T., 2012, in Takahashi T., Murray S. S., den Herder J.-W. A.eds, Proc. SPIE Conf. Ser. Vol. 8443, Space Telescopes and Instrumentation 2012: Ultraviolet to Gamma Ray. SPIE, Bellingham, p. 844313
Gendreau K. C. et al., 2016, in den Herder J.-W. A., Takahashi T., Bautz M.eds, Proc. SPIE Conf. Ser. Vol. 9905, Space Telescopes and Instrumentation 2016: Ultraviolet to Gamma Ray. SPIE, Bellingham, p. 99051H
Gilfanov M., 2010, in Belloni T.ed., Lecture Notes in Physics, Vol. 794. Springer-Verlag, Berlin, p. 17
Haardt F., Maraschi L., 1993, ApJ, 413, 507
Jana A., Naik S., Chatterjee D., Jaisawal G. K., 2021, MNRAS, 507, 4779
Kislat F., Clark B., Beilicke M., Krawczynski H., 2015, Astropart. Phys., 68, 45
Kosenkov I. A. et al., 2020, MNRAS, 496, L96
Krawczynski H., Beheshtipour B., 2022, ApJ, 934, 4
Krawczynski H. et al., 2022, Science, 378, 650
Kushwaha A., Jayasurya K. M., Agrawal V. K., Nandi A., 2023, MNRAS, 524, L15
Leong C., Kellogg E., Gursky H., Tananbaum H., Giacconi R., 1971, ApJ, 170, L67
Majumder S., Kushwaha A., Das S., Nandi A., 2024, MNRAS, 527, L76
Manfreda A., 2020, J. Instrum., 15, C04049
Méndez M., van der Klis M., 1997, ApJ, 479, 926
Motta S., Homan J., Muñoz Darias T., Casella P., Belloni T. M., Hiemstra B., Méndez M., 2012, MNRAS, 427, 595
Orosz J. A., Steiner J. F., McClintock J. E., Buxton M. M., Bailyn C. D., Steeghs D., Guberman A., Torres M. A. P., 2014, ApJ, 794, 154
Podgorný J., Dovčiak M., Marin F., Goosmann R., Różańska A., 2022, MNRAS, 510, 4723
Podgorný J. et al., 2023, MNRAS, 526, 5964
Poutanen J., Svensson R., 1996, ApJ, 470, 249
Poutanen J., Veledina A., Beloborodov A. M., 2023, ApJ, 949, L10
Ratheesh A. et al., 2023, ApJ, 964, 77
Rawat D., Garg A., Méndez M., 2023a, MNRAS, 525, 661
Rawat D., Garg A., Méndez M., 2023b, ApJ, 949, L43
Remillard R. A., McClintock J. E., 2006, ARA&A, 44, 49
Rodriguez Cavero N. et al., 2023, ApJ, 958, L8
Romano P. et al., 2006, A&A, 456, 917
Schnittman J. D., Krolik J. H., 2009, ApJ, 701, 1175
Schnittman J. D., Krolik J. H., 2010, ApJ, 712, 908
Shakura N. I., Sunyaev R. A., 1973, A&A, 24, 337
Smale A. P., Boyd P. T., 2012, ApJ, 756, 146
Sobolev V. V., 1963, A Treatise on Radiative Transfer. Van Nostrand, Princeton, NJ
Steiner J. F., McClintock J. E., Orosz J. A., Remillard R. A., Bailyn C. D., Kolehmainen M., Straub O., 2014, ApJ, 793, L29
Stern B. E., Poutanen J., Svensson R., Sikora M., Begelman M. C., 1995, ApJ, 449, L13
Svoboda J. et al., 2024, ApJ, 960, 3
Taverna R., Zhang W., Dovčiak M., Bianchi S., Bursa M., Karas V., Matt G., 2020, MNRAS, 493, 4960
Tomaru R., Done C., Odaka H., 2023, MNRAS, 527, 7047
Torpin T. J., Boyd P. T., Smale A. P., Valencic L. A., 2017, ApJ, 849, 32
Verner D. A., Ferland G. J., Korista K. T., Yakovlev D. G., 1996, ApJ, 465, 487
Weisskopf M. C. et al., 2022, J. Astron. Telesc. Instrum. Syst., 8, 026002
White N. E., Marshall F. E., 1984, ApJ, 281, 354
Wilms J., Allen A., McCray R., 2000, ApJ, 542, 914
Wilms J., Nowak M. A., Pottschmidt K., Heindl W. A., Dove J. B., Begelman M. C., 2001, MNRAS, 320, 327
Zhang W., Dovčiak M., Bursa M., 2019, ApJ, 875, 148

This paper has been typeset from a TEX/LATEX file prepared by the author.